

Measurement and calibration method for an optical encoder based on adaptive differential evolution-Fourier neural networks

This article has been downloaded from IOPscience. Please scroll down to see the full text article.

2013 Meas. Sci. Technol. 24 055007

(<http://iopscience.iop.org/0957-0233/24/5/055007>)

View [the table of contents for this issue](#), or go to the [journal homepage](#) for more

Download details:

IP Address: 211.68.3.224

The article was downloaded on 26/04/2013 at 01:22

Please note that [terms and conditions apply](#).

Measurement and calibration method for an optical encoder based on adaptive differential evolution-Fourier neural networks

Fang Deng^{1,2}, Jie Chen^{1,2}, Yanyong Wang^{1,2,3} and Kun Gong^{1,2}

¹ School of Automation, Beijing Institute of Technology, Beijing, People's Republic of China

² Key Laboratory of Intelligent Control and Decision of Complex Systems, Beijing, People's Republic of China

³ China North Vehicle Research Institute, Beijing, People's Republic of China

E-mail: dengfang@bit.edu.cn

Received 13 July 2012, in final form 6 March 2013

Published 4 April 2013

Online at stacks.iop.org/MST/24/055007

Abstract

A high-precision measurement and calibration device is proposed in this paper. The resolution of this device can reach 18 binary bits, and it can measure whether or not optical encoders reach their nominal accuracy. The method based on the adaptive differential evolution-Fourier neural network (ADE-FNN) is proposed to improve the accuracy of optical encoders. This method makes full use of the FNN to establish an error compensation model for optical encoders and introduces an ADE algorithm to optimize the weights of the FNN. Compared to a nonlinear least-squares method, a back propagation neural network and a standard FNN, this method possesses many advantages, such as the fine nonlinear approximation capability, faster convergence speed and easiness of finding the global optimum. Experimental results demonstrate that after being calibrated by this method, significant improvement regarding the accuracy of optical encoders can be achieved.

Keywords: optical encoder, adaptive differential evolution, Fourier neural network, calibration

(Some figures may appear in colour only in the online journal)

1. Introduction

An optical encoder is a kind of angular sensor, as shown in figure 1, which is an opto-mechanical-electronic device transforming a light distribution into two sinusoidal electrical signals that can be used to define the relative position between a reading head and an angular scale [1, 2]. By virtue of high accuracy, wide measurement range, high response frequencies, light weight and high resolution, optical encoders have been widely used in modern military, aerospace, bioscience and other precision applications [3, 4].

To improve the accuracy of the optical encoder two factors to be considered are as follows:

- product inspection is necessary to make sure that the actual accuracy of optical encoders satisfies design specifications;
- recalibration is compulsory to guarantee that optical encoders maintain the nominal accuracy, affected by mechanical wear and corrosion, and ageing of electronic components after a period of operation.

In the existing literature, the accuracy of optical encoders is measured by means of other higher accuracy angular sensors which are used as a benchmark for angular measurement. In [5], a regular 23-faced polygon is chosen as the benchmark, a high-precision rotary table controls the rotation of an optical encoder and data are acquired when the photoelectric collimator is perpendicular to one face of the polygon. Although this equipment can guarantee higher measurement



Figure 1. Optical encoders.

accuracy, it has the drawbacks of low automation, high cost and complex operation. Meanwhile, the resolution of this equipment is restricted by the number of faces of the polygon as well. On the basis of [5], the upgraded equipment described in [6] can automatically acquire the readout of the encoder. In [7], a calibration device is described comprising an inner rotary table, an outer rotary table, an electronic autocollimator and an irregular five-faced polygon featuring high-quality faces. The polygon is mounted on the inner rotary table while the autocollimator is placed on the outer rotary table. During the measurement, the rotational axes of the two rotary tables should be regulated to be congruent. There exist many careful adjustments so that the pyramidal error of this polygon may be minimized or omitted. Such equipment cannot be generalized because of the high cost of the rotary table and the polygon.

No matter how well optical encoders are designed and fabricated, their actual accuracies do not match the nominal accuracy. Therefore, much effort has been made to find an effective and feasible software-based calibration method [8] to improve the accuracy of optical encoders. The nonlinear least-squares method (LS) was adopted to compensate the encoder's circular grating error [9]. It has many shortcomings, such as strong dependence on uniform sampling and large sample data, complex operations and easiness of being influenced by the size of training data. The back propagation (BP) neural network method with hybrid modeling adopting the 8:20:6 model (8 inputs, 20 hidden nodes and 6 outputs) was employed in [10, 11] to improve the calibration precision, which adopts the sigmoid activation function and Levenberg–Marquardt (LM) algorithm to train the network. It can approximate nonlinear mapping relationships without uniform sampling. However, inevitably, BP has some obvious limitations. The convergence speed is very slow or even non-existent and the algorithm may fall into any local minimum. A combination of the sine function and particle swarm optimization (PSO) was proposed, improving the measurement accuracy of circular grating angle sensors [12].

For the drawbacks of the above methods, novel methodologies are required to solve the aforementioned problems. This is the motivation for the upgraded measurement and calibration device (MCD) and a novel hybrid calibration method based on the adaptive differential evolution (ADE) algorithm and Fourier neural network (ADE-FNN). The FNN, whose activation function is an orthogonal Fourier series, is used to model the optical encoder error, and the ADE algorithm is introduced to train the FNN's weights. The main features of this hybrid method are summarized as follows.

Table 1. Description of main components.

Item	Description
MCU	4 kB RAM
PC	2 GB RAM, Core i3 processor
Stepping motor	Three-phase, step angle 0.6°
Stepping motor driver	Three-phase hybrid driver
Worm reduction gear	Reduction ratio:109

- The FNN is easy to realize and can approximate nonlinear mapping relationships at an arbitrary accuracy [13, 14].
- The FNN with an orthogonal Fourier series transforms a nonlinear optimization problem into a linear optimization problem, which significantly improves the convergence speed and effectively avoids local minima.
- The FNN is easy to realize both in computing and hardware, because the structure of the FNN is limited by system bandwidth and clear physical meaning. Each neuron can be regarded as the frequency filter of the respective frequency component, so that the network structure is limited by the system bandwidth. All the nonlinearities and uncertainties of the dynamical system are lumped together and iteratively compensated by the FNN so that *a priori* knowledge of the system model is not required [15].
- The FNN's initial weights, calculated by the ADE algorithm, do not rely on the system's prior knowledge.
- The FNN has high precision and strong generalization ability. The calibration operation without uniform sampling is very simple.

This paper is organized as follows. In section 2, we briefly elaborate the skeleton of the special MCD. Section 3 describes the structure and learning algorithm of the ADE-FNN. Section 4 provides different criteria to evaluate the measurement accuracy of optical encoders. In section 5, the ADE-FNN is used to improve the accuracy of optical encoders, measured by the MCD, which do not reach their nominal accuracy. Conclusions are summarized in section 6.

2. Measurement and calibration device

The experimental data are collected by the MCD which is an electromechanical device. In 2007, the prototype was devised by Deng *et al* [16]. The upgraded device is introduced in this paper, as shown in figure 2.

2.1. Hardware configuration

The structure of the MCD is shown in figure 3, and the description of the main components is listed in table 1. Step angles of 1/8, 1/4, 1/2 and 1/1 can be chosen on the stepping motor driver. The angular sensor is required to measure and calibrate in the following experiments.

The resolution of the MCD can be calculated by the following equation:

$$R_{\text{dev}} = SS_{nd}F_c/R_r, \quad (1)$$

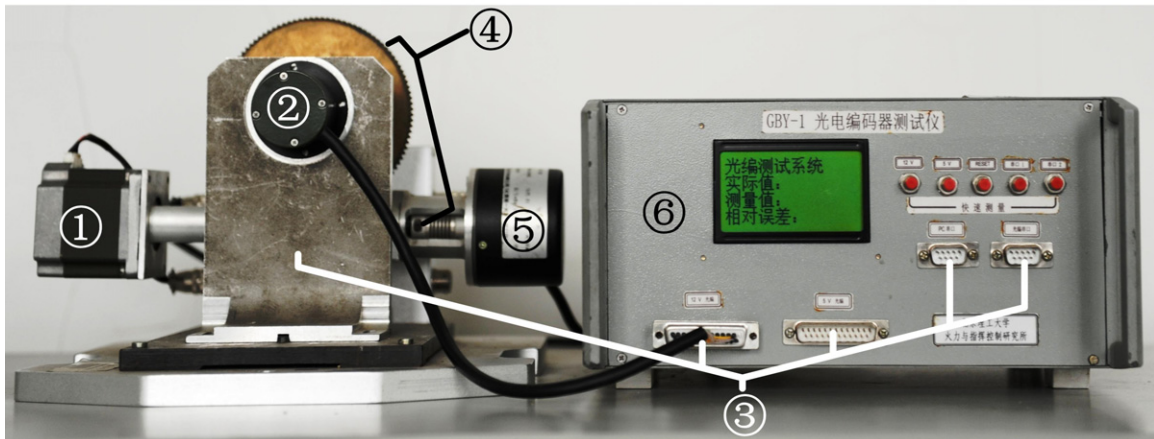


Figure 2. The MCD made for measuring and calibrating optical encoders. ① Stepping motor, ② angular sensor, ③ multi-interface, ④ worm reduction gear, ⑤ incremental encoder, ⑥ control box (including the MCU and motor driver).

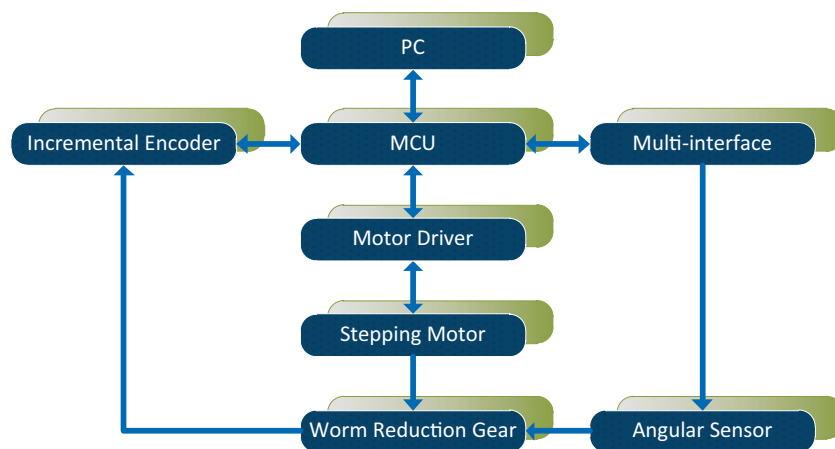


Figure 3. The MCD structure.

where R_{dev} is the resolution of the MCD, S is the step angle of the stepping motor, S_{nd} is the number of micro-step divisions (1/8, 1/4, 1/2 or 1/1), F_c is the conversion factor (3600 here) and R_r is the reduction ratio. Numerically, $R_{dev} = 2.48''$.

2.2. Software architecture

The software architecture of the MCD is shown in figure 4. There are two parts: MCU software and PC software.

2.2.1. MCU software. MCU software is developed to control the rotation of the stepping motor according to the parameter setting in the human-computer interaction interface, collect the output of the optical encoder, as well as communicate with the PC. The monitoring module monitors the stepping motor by reading the incremental optical encoder.

2.2.2. PC software. The rotation information, such as the rotation direction and rotation intervals per step, is set in the human-computer interaction interface. Experimental data are processed and analyzed in the data processing module. Furthermore, the error value, the mean value and the variance of each experimental datum can be automatically calculated (the detailed calculation formulae can be found in section 4).

The calibration module can improve the accuracy of optical encoders which do not reach their nominal accuracy. The kernel of the calibration module is the ADE-FNN (more details can be found in section 3).

3. Adaptive differential evolution algorithm and Fourier neural network

This section introduces the architecture and the learning algorithm of the ADE-FNN, which is a kind of feed-forward neural network. Since the initial values of the FNN's weights are difficult to choose, here we propose the ADE algorithm which can effectively train the FNN's weights.

This paper introduces the ADE-FNN into the calibration of optical encoders. The input-output relationship of an optical encoder can be expressed by

$$x = g(z), \tag{2}$$

where z is the measured physical quantity and x is the output of the optical encoder. Ideally, $g(z)$ is a linear function. However, this function is nonlinear in practice because of the installation error, ageing of electronic components, etc.

The calibration block diagram of optical encoders is shown in figure 5. The ADE-FNN is employed to establish

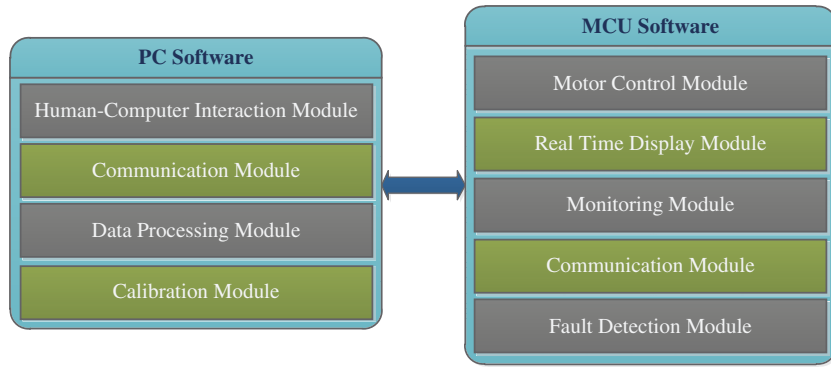


Figure 4. Software architecture.

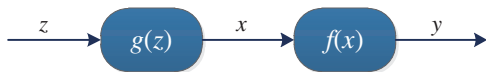


Figure 5. The structure of calibration.

the inverse model $f(x)$ [17]. The ideal result is that optical encoders calibrated by ADE-FNN can present linear characteristics ($y = z$).

3.1. Fourier series

To aid a better comprehension of the FNN, Fourier series will be briefly outlined in this subsection.

The function $y = f(x)$ with the period T can be expressed with the Fourier series as follows:

$$y = a_0 + \sum_{n=1}^{\infty} \left(a_n \cos \frac{2n\pi x}{T} + b_n \sin \frac{2n\pi x}{T} \right), \quad (3)$$

$$a_0 = \frac{1}{T} \int_0^T f(x) dx, \quad (4)$$

$$a_n = \frac{2}{T} \int_0^T f(x) \cos \frac{2n\pi x}{T} dx, \quad n = 1, 2, 3, \dots, \infty, \quad (5)$$

$$b_n = \frac{2}{T} \int_0^T f(x) \sin \frac{2n\pi x}{T} dx, \quad n = 1, 2, 3, \dots, \infty, \quad (6)$$

where a_0 , a_n and b_n are the Fourier coefficients. $\{1, \cos \frac{2\pi x}{T}, \sin \frac{2\pi x}{T}, \cos \frac{4\pi x}{T}, \sin \frac{4\pi x}{T}, \dots, \cos \frac{2n\pi x}{T}, \sin \frac{2n\pi x}{T}, \dots\}$ is the set of triangular orthogonal function bases of the Fourier series.

3.2. Fourier neural network

Assume that the FNN under consideration has a single input and a single output (SISO). It is well known that neural networks with one hidden layer are ample for approximating functions that are defined in [13, 14, 18]. For this reason, the FNN shown in figure 6 is a three-layer network consisting of nodes and directional weighted links through which nodes are linked. Let O_i^j denote the output of the i th node in the j th layer.

Layer 1. The node in this layer sends the input variable x out, and the weights between layer 1 and layer 2 are all equal to 1:

$$O_1^1 = x. \quad (7)$$

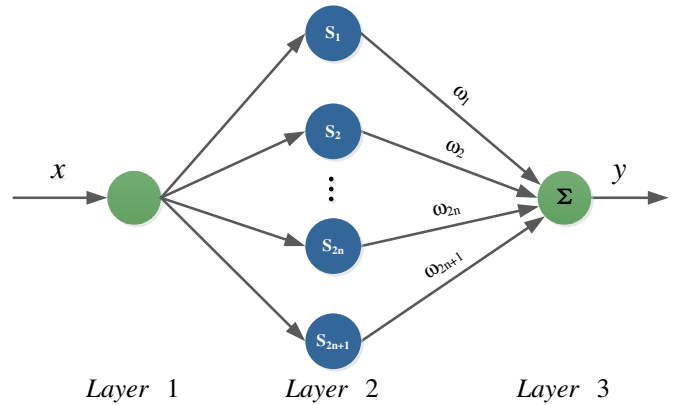


Figure 6. The structure of the SISO FNN.

Layer 2. This layer is the so-called hidden layer. Every node k in layer 2 has a node function, as shown in equation (8):

$$O_k^2 = S_k \omega_k, \quad k = 1, 2, 3, \dots, 2n + 1. \quad (8)$$

Every node in this layer has an activation function S_k , such as the sigmoid function and the Gaussian function. Here, the expressions of activation functions are shown in equation (9), namely triangular orthogonal function bases of the Fourier series:

$$\begin{cases} S_1 = 1, \\ S_{2h} = \cos \frac{2h\pi x}{T}, \\ S_{2h+1} = \sin \frac{2h\pi x}{T}. \end{cases} \quad h = 1, 2, 3, \dots, n, \quad (9)$$

Furthermore, the weights ω_k ($k = 1, 2h, 2h + 1$) between layer 2 and layer 3 are represented by the following equation:

$$\begin{cases} \omega_1 = a_0, \\ \omega_{2h} = a_h, \\ \omega_{2h+1} = b_h, \end{cases} \quad (10)$$

where a_0 , a_h and b_h are the Fourier coefficients.

Layer 3. In this layer, there is only a single node. The label Σ denotes the sum of the outputs of layer 2, i.e.

$$O_1^3 = \sum_{k=1}^{2n+1} O_k^2 \quad (11)$$

$$= \sum_{k=1}^{2n+1} S_k \omega_k \quad (12)$$

$$= S_1\omega_1 + \dots + S_{2n}\omega_{2n} + S_{2n+1}\omega_{2n+1} \quad (13)$$

$$= a_0 + \dots + a_n \cos \frac{2n\pi x}{T} + b_n \sin \frac{2n\pi x}{T} \quad (14)$$

$$= a_0 + \dots + \sum_{h=1}^n \left(a_h \cos \frac{2h\pi x}{T} + b_h \sin \frac{2h\pi x}{T} \right). \quad (15)$$

The aim of the training is to iteratively reduce the error between the target value and the predicted value. There is an unaccounted-for rule for selecting the most appropriate error measure (or energy) function [19]. For simplicity, the squared error E is used, as defined by the following equation:

$$E = \frac{1}{2} \sum_{i=1}^M e_i^2, \quad (16)$$

$$e_i = Y_i - y_i, \quad i = 1, 2, 3, \dots, M, \quad (17)$$

where Y_i is the i th output value of the FNN, y_i is the i th desired output value of an optical encoder (measured physical quantity) and M is the size of the training sample.

From the above description, we can find that equations (14) and (3) are equivalent [20]. The output of the FNN is the anterior $2n + 1$ items of the Fourier series and the number of nodes in layer 2 increases (or decreases) in pairs. There exists no exact method to determine the number of nodes in each hidden layer [21]. Some articles [13, 22, 23] have given some methods and empirical formulae to obtain the preliminary number of hidden layer nodes. We give an empirical formula to select the preliminary n according to the papers [22, 23]:

$$n = 2\sqrt{(N_O + 2)M}, \quad (18)$$

where N_O is the size of the output neurons and M is the size of the training sample. The structure of the used FNN is determined by increasing the number of FNN nodes until no further improvement of accuracy can be observed. It means that a larger n brings a higher fitting accuracy with the side effect that the training time will rapidly increase, and this may have the risk of overfitting.

The original mapping relationship between the inputs and outputs of the FNN is nonlinear. However, the output of the FNN is a linear combination of all nodes' output in layer 2. So, a nonlinear optimization problem is transformed into a linear optimization problem by the FNN with a triangular orthogonal activation function. This key transformation must considerably improve the convergence speed and avoid being trapped in local minima.

Unfortunately, it is time-consuming and formidable to choose initial weights of the FNN. Moreover, the convergence speed depends on the initial weights. Here, we introduce an ADE algorithm, as discussed in subsection 3.3, which can quickly and effectively train the FNN's weights and overcome the difficulty of choosing the initial weights.

3.3. Adaptive differential evolution algorithm

The differential evolution (DE) algorithm, put forward by Storn and Price [24], is a new heuristic method for the global

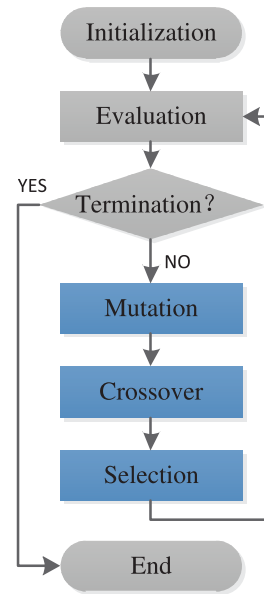


Figure 7. Flowchart of the ADE algorithm.

optimization over continuous spaces. A flowchart of the DE algorithm is shown in figure 7.

The pressing task derived from the FNN, consisting of parameter $D = 2n + 1$, can be represented by a D -dimensional vector. A population at each generation G is composed of NP D -dimensional parameter vectors $\mathbf{p}_{i,G}, i = 1, 2, 3, \dots, NP$. NP is a constant integer $\in [5D, 10D]$. The initial population is randomly generated, and the population is optimized by executing the loop of the mutation, crossover and selection operations.

Mutation. For each target vector $\mathbf{p}_{i,G}$, a mutant vector is produced as follows:

$$\mathbf{v}_{i,G+1} = \mathbf{p}_{r_1,G} + F \cdot (\mathbf{p}_{r_2,G} - \mathbf{p}_{r_3,G}), \quad (19)$$

where $i, r_1, r_2, r_3 (i \neq r_1 \neq r_2 \neq r_3) \in [1, 2, 3, \dots, NP]$ are randomly chosen, and F is the scaling factor with $F \in [0, 2]$. To satisfy the condition that these four indices are mutually different, the NP should be greater than or equal to 4.

Crossover. For the purpose of enriching the diversity of the perturbed parameter vectors, a binomial crossover is used [24]. A trial vector can be generated in the following way:

$$u_{i,G+1} = u_{j,i,G+1} = \begin{cases} v_{j,i,G+1} & \text{if randb}(j) \leq \text{CR} \\ & \text{or } j = \text{rnbr}(i), \\ p_{j,i,G} & \text{if randb}(j) > \text{CR} \\ & \text{and } j \neq \text{rnbr}(i), \end{cases} \quad (20)$$

where $j = 1, 2, 3, \dots, n$, $\text{randb}(j) \in [0, 1]$ is the j th evaluation of a uniform random number and $\text{rnbr}(i) \in [1, 2, 3, \dots, n]$ is a randomly chosen index. CR is the crossover rate with $\text{CR} \in [0, 1]$, which has to be determined by the user in the standard DE algorithm. If CR is more than or equal to the random number $\text{randb}(j)$, the trial parameter is inherited from the mutant, $v_{j,i,G+1}$; otherwise, the parameter is copied from the vector, $p_{j,i,G}$. So it is conducive to maintaining the diversity of the population while the population does not easily produce a new individual.

So, we introduce the following strategy to regulate CR adaptively (see equation (21)):

$$CR_i = CR_{\min} + (CR_{\max} - CR_{\min}) \frac{f_i - f_{\min}}{f_{\max} - f_{\min}}, \quad (21)$$

where CR_i is the crossover constant of the i th individual, CR_{\min} and CR_{\max} are the minimum and maximum crossover constants, respectively. f_i is the fitness of the i th individual, f_{\min} is the minimum and f_{\max} is the maximum individual fitness in the current population.

Then, for individuals with lower fitness, a larger CR will increase the contribution of the mutant vector to the trial vector and accelerate the elimination of these individuals. For individuals with higher fitness, a smaller CR will favor them being retained in the population at generation $G + 1$.

Selection. The trial vector $u_{i,G+1}$ will be compared with the target vector $p_{i,G}$ to determine whether or not it becomes a member of the population at generation $G + 1$ according to the cost function (see equation (16)):

$$p_{i,G+1} = \begin{cases} u_{i,G+1} & \text{if } E(u_{i,G+1}) < E(p_{i,G}), \\ p_{i,G} & \text{otherwise.} \end{cases} \quad (22)$$

We utilized ADE mentioned above to optimize the weights of the FNN. Although it is very useful in the optimization problem, there is no proof of convergence of this method.

4. Approximation accuracy evaluation

To evaluate the measurement accuracy of optical encoders, different criteria are used. The standard deviation of the error (STD) criterion, the max absolute error (MaxAbs) criterion and the mean absolute error (MeanAbs) are defined as follows.

The system accuracy given in the specifications of optical encoders is usually expressed by the STD. The STD criterion is given by

$$STD = \left[\sum_{i=1}^M (e_i - \bar{e}_i)^2 / (M - 1) \right]^{1/2}, \quad (23)$$

$$e_i = \hat{x}_i - z_i, \quad (24)$$

$$\bar{e}_i = \frac{1}{M} \sum_{i=1}^M e_i, \quad (25)$$

where \hat{x}_i is the i th output value of an optical encoder (or a network), and M and z are defined in section 3.

The MaxAbs criterion is given by

$$MaxAbs = \max\{|e_i|, i = 1, 2, 3, \dots, M\}. \quad (26)$$

The MeanAbs criterion is given by

$$MeanAbs = \frac{1}{M} \sum_{i=1}^M |e_i|. \quad (27)$$

5. Experimental results

5.1. Device clearance measurement

The clearance measurement is executed to examine the clearance of the MCD. Firstly, the stepping motor is set to rotate in the counterclockwise direction with the specified

Table 2. Results of clearance measurement.

Item	Angle (deg)	Rotation angle (deg/interval)
1	282.56	8.01
2	274.55	8.00
3	266.55	7.99
4	258.56	0
5	266.55	7.99
6	274.55	8.00
7	282.56	8.01

Table 3. Main specifications of optical encoders.

Item	En-A	En-B
Resolution	19.8"	39.6"
Positions per revolution	65 536 (16 bits)	32 768 (15 bits)
System accuracy	40"	40"
Measurement range	360°	360°

rotation angle. Then the motor rotates in the clockwise direction with the counterpart specified rotation angle. In this experiment, we set the specified rotation angle to be 8° per interval and the measurement results of the MCD rotation angle are listed in table 2. It is able to conduct the clearance measurement in the reverse order (first clockwise, and then anticlockwise). So the clearance of the MCD can be negligible.

5.2. Measurement experiment

Measurement experiments with optical encoders are performed for the purpose of determining whether or not optical encoders can reach their claimed accuracy. Optical encoders En-A and En-B are customized for our laboratory by research institutes A and B, and some of the main specifications are shown in table 3. En-A and En-B are mounted on the MCD introduced in section 2, and we test En-A and En-B successively.

The measurement procedure involves the rotation angle, the number of measurement points as well as the rotation direction. The rotation angle is set to 10° per interval. This means that the interval between the adjacent outputs of an optical encoder should be equal to 10° throughout the measurement process. Thus 36 measurement points should be collected in the full measurement range. The measurement experiments were carried out on the same day and the same location when the stepping motor was set to rotate in the clockwise direction.

Figure 8(a) indicates that the interval of En-A is not equal to the specified rotation angle in magnitude, and the interval curve is a deformed circle shape. So it can be visually determined that the accuracy of En-A is very low. In figure 9(a), the interval curve of En-B is an approximate circle. Relatively speaking, En-B is more accurate than En-A. Absolute error curves of En-A and En-B are shown in figures 11 and 12, respectively. Table 4 shows the measuring results in different evaluation forms. The MaxAbs and MeanAbs of En-A are 3.61° and 1.6844°, respectively. With regard to the STD, En-A with a specification accuracy of 40" and En-B are less accurate than their nominal accuracy.

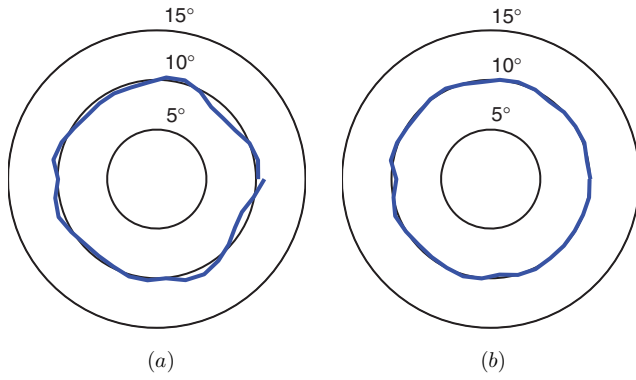


Figure 8. Radar chart of the interval: (a) the interval of uncalibrated En-A, (b) the interval of En-A calibrated by ADE-FNN.

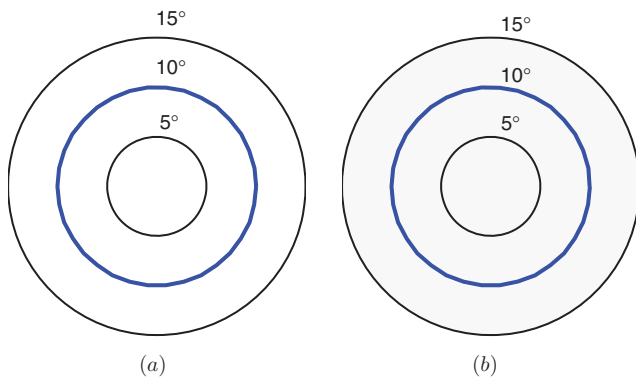


Figure 9. Radar chart of the interval: (a) the interval of uncalibrated En-B, (b) the interval of En-B calibrated by ADE-FNN.

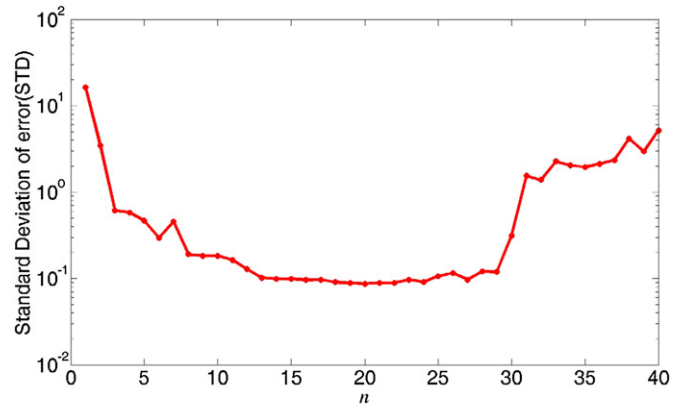
Table 4. Results of measurement.

Item	En-A (deg)	En-B (deg)
Measured STD	1.0712	0.03
MaxAbs	3.61	0.34
MeanAbs	1.6844	0.2964

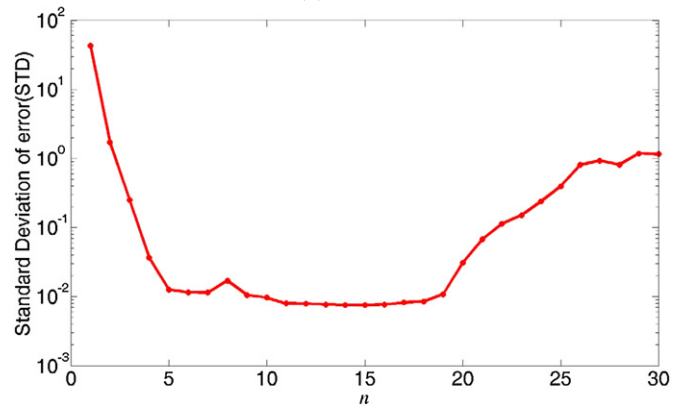
5.3. Calibration experiment

In order to improve the accuracy of En-A and En-B, some calibration experiments are performed. That the repeatability of optical encoders under consideration is good is shown by repeating the same measurement experiments over a period of time. Generally speaking, system errors and random errors coexist in any measurement, and repeatability error belongs to the random error in nature [25]. So, an arbitrary and simple conclusion is that the system errors of En-A and En-B are greater than random errors and the major reason for their low accuracy is the system error which includes the quality of the graduation, the eccentricity of the graduation to the bearings, the elasticity of the encoder shaft and its coupling with the drive shaft, etc [26]. The system error can be amended through calibration [8].

The proposed ADE-FNN has been applied to calibrate En-A and En-B. The relationship between STD and n is shown in figure 10. The figure shows that a larger n brings a higher fitting accuracy, but when n increases to a certain degree, we face the risk of overfitting.



(a) En-A



(b) En-B

Figure 10. The relationship between the STD error and n .

Table 5. Parameter settings for the ADE-FNN.

Item	En-A	En-B
T	360	360
G	20 000	20 000
D	41	31
NP	205	155
F	0.53	0.59
CR_{min}	0	0
CR_{max}	1	1

Parameter settings for the ADE-FNN are listed in table 5. Since all optical encoders will not possess exactly the same error characteristics due to inherent differences in their manufacture, the ADE-FNN is successively trained on one error curve. Consequently, there are two different sets of ADE-FNN weights which are used to compensate the system errors of En-A and En-B, respectively. The ADE-FNN was tested with respective test data files comprising 36 resolved angle values each, which were the data of another group and not used during the training of the network.

The reduction of the STD of En-A is from 1.0712° (pre-calibration) to 0.0882° (= 317.52'') (post-calibration). However, it still does not achieve its nominal accuracy. The error range of En-B narrows significantly, and its STD decreases to 0.0076° (= 27.36''). Thus En-B calibrated by the ADE-FNN is slightly more accurate than its nominal accuracy. Figures 8(b) and 9(b) show the radar charts of the intervals of En-A and En-B calibrated by the ADE-FNN, which are more

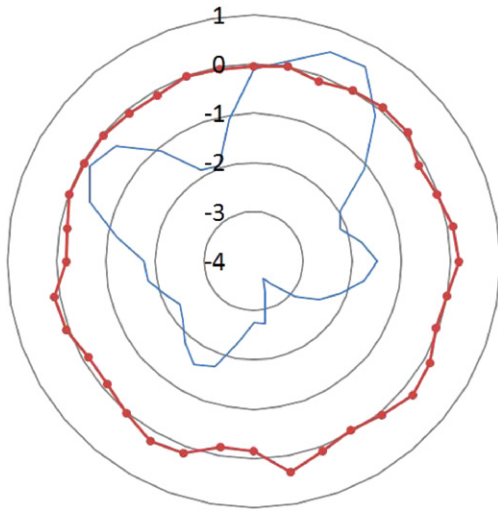


Figure 11. Comparison of the absolute error between uncalibrated and calibrated En-A. Solid line—the absolute error of uncalibrated En-A, solid line with dots—the absolute error of En-A calibrated by ADE-FNN.

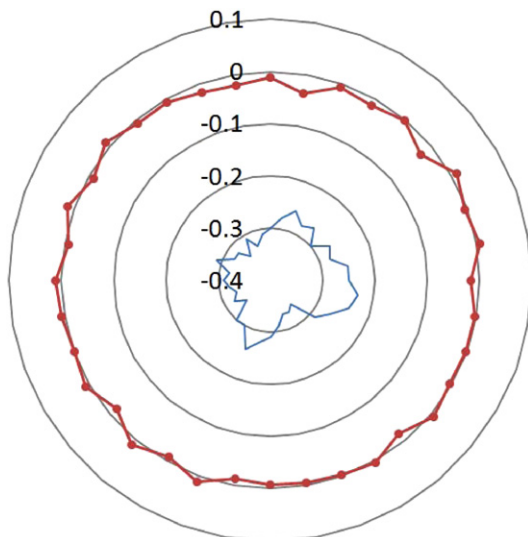


Figure 12. Comparison of the absolute error between uncalibrated and calibrated En-B. Solid line—the absolute error of uncalibrated En-B, solid line with dots—the absolute error of En-B calibrated by ADE-FNN.

round than before calibration. Figures 11 and 12 show the absolute error curves of the two optical encoders calibrated by the ADE-FNN. The closer the curve approaches the circle marked with 0, the smaller the absolute error. The accuracy of En-A and En-B calibrated by the ADE-FNN has been improved obviously.

Finally, a comparative study including standard FNN, BP and LS is conducted to illustrate the effectiveness of the proposed method and the standard FNN utilizing the LM algorithm to train data. BP used the standard BP network with 19 nodes (which is the best one either for En-A or En-B) in the hidden layer and the LM algorithm to train. We used the same experimental data as the training data, and used the data of another group, which were not used during the training of the network, to test the results of compensation. Parameter settings

Table 6. Parameter settings for the FNN and BP.

Item	En-A		En-B	
	FNN	BP	FNN	BP
The number of nodes in the hidden layer	41	19	65	19
Maximum number of epochs	20 000	20 000	20 000	20 000
Sum-squared error goals	10^{-5}	10^{-5}	10^{-7}	10^{-7}

Table 7. Comparative STD, MaxAbs and MeanAbs results of En-A calibrated by the ADE-FNN, FNN, BP and LS.

Item	STD (deg)	MeanAbs (deg)	MaxAbs (deg)
ADE-FNN	0.0882	0.1694	0.3213
FNN	0.1306	0.1813	0.3909
BP	0.3086	0.1901	1.1804
LS	0.5956	0.4984	1.3419

Table 8. Comparative STD, MaxAbs and MeanAbs results of En-B calibrated by the ADE-FNN, FNN, BP and LS.

Item	STD (deg)	MeanAbs (deg)	MaxAbs (deg)
ADE-FNN	0.0076	0.0101	0.0206
FNN	0.0104	0.0101	0.0246
BP	0.0185	0.0163	0.0840
LS	0.0222	0.0176	0.0436

for the ADE-FNN are listed in table 5 and parameter settings for the FNN and BP are listed in table 6. For the ADE-FNN and the other three methods, the results presented in tables 7 and 8 clearly show that the ADE-FNN is the only effective calibration method that could improve the accuracy of optical encoders in terms of the STD criterion, MaxAbs criterion and MeanAbs criterion. Because there are some random factors in calculation, the results shown in tables 7 and 8 are the averages of 100 times numerical calculation.

6. Conclusions

This paper introduces a useful device which is in charge of measuring and calibrating optical encoders and a novel modeling method based on the FNN trained by ADE. Then, this method was carried out to calibrate two optical encoders for the sake of demonstrating its feasibility and usefulness.

The experimental results show that the ADE-FNN is superior to the standard FNN, BP and LS methods in terms of the STD criterion, MaxAbs criterion and MeanAbs criterion. Besides, the ADE-FNN has the advantages of strong approximation capability, fast convergence speed, robustness to initial weights, does not easily fall into local minimum, simple operations and small network scale. From our experiments, the ADE-FNN reaffirms its suitability as an excellent method for the calibration of optical encoders.

The calibration experiments on optical encoders are implemented on the premise of good repeatability. However, it is a prerequisite that data filtering is required to reduce the effect of random error on the experimental data when optical encoders have unsatisfied repeatability.

Acknowledgments

This work is supported by National Science Fund for Distinguished Young Scholars of China (grant no. 60925011), Projects of Major International (Regional) Joint Research Program NSFC (grant no. 61120106010) and Provincial Key Fund of China (grant no. 9140A07010511BQ0105).

References

- [1] Sanchez-Brea L M and Morlanes T 2008 Metrological errors in optical encoders *Meas. Sci. Technol.* **19** 115104
- [2] Ye S X 2003 *Photoelectric Precise Metrology of Displacement* (Chengdu: Sichuan Science and Technology Press) (in Chinese)
- [3] Tobita K, Ohira T, Kajitani M, Kanamori C, Shimojo M and Ming A 2005 A rotary encoder based on magneto-optical storage *IEEE/ASME Trans. Mechatronics* **10** 87–97
- [4] Hane K, Endo T, Ito Y and Sasaki M 2001 A compact optical encoder with micromachined photodetector *J. Opt. A: Pure Appl. Opt.* **3** 191–5
- [5] Li G Y, Cao L, Sheng J M, Chen J Q, Ma J F, Cai Q Y, Zhao L and Shan Y N 1990 Measurement and application of photoelectric encoder *Mech. Des.* **7** 57–8 (in Chinese)
- [6] Geckeler R D, Fricke A and Elster C 1990 Calibration of angle encoders using transfer functions *Meas. Sci. Technol.* **17** 2811–8
- [7] Han X D 2002 An angular displacement sensor photoelectric detector *Chinese Patent* 01138860.9
- [8] Dhar V K, Tickoo A K, Kaul S K, Koul R and Dubey B P 2010 Artificial neural network-based error compensation procedure for low-cost encoders *Meas. Sci. Technol.* **21** 015112
- [9] Zhang L S and Guan B L 2007 Error correction and its application to multi-joint CMM research *Metrol. Meas. Technol.* **27** 41–4 (in Chinese)
- [10] Xie S L, Chen S L, Zhang X N and Zhu C C 2010 Hybrid neural network models of transducers *J. Mech. Eng.* **46** 6–15 (in Chinese)
- [11] Xie S L, Zhang X N, Chen S L and Zhu C C 2011 Hybrid neural network models of transducers *Meas. Sci. Technol.* **22** 105201
- [12] Gao G B, Wang W, Lin K and Chen Z C 2010 Error compensation and parameter identification of circular grating angle sensors *Opt. Precis. Eng.* **18** 1766–71 (in Chinese)
- [13] Hecht-Nielsen R 1987 Kolmogorov's mapping neural network existence theorem *Proc. IEEE Int. Conf. on Neural Networks* vol 3 pp 11–3
- [14] Lippmann R P 1987 An introduction to computing with neural nets *IEEE ASSP Mag.* **4** 4–22
- [15] Zuo W, Zhu Y and Cai L L 2009 Fourier-neural-network-based learning control for a class of nonlinear systems with flexible components *IEEE Trans. Neural Netw.* **20** 139–51
- [16] Deng F, Chen J, Chen W J and Chi C 2007 A high precision test method and apparatus for photoelectric encoder *Trans. Beijing Inst. Technol.* **27** 977–80 (in Chinese)
- [17] Marconato A, Hu M Q, Bori A and Petri D 2008 Dynamic compensation of nonlinear sensors by a learning-from-examples approach *IEEE Trans. Instrum. Meas.* **57** 1689–94
- [18] White H 1989 Learning in artificial neural networks: a statistical perspective *Neural Comput.* **1** 425–64
- [19] Jang J R 1993 ANFIS: Adaptive-network-based fuzzy inference system *IEEE Trans. Syst. Man Cybern.* **23** 665–85
- [20] Yang X H, Dai H P and Sun Y X 2003 SIMO Fourier neural networks research *Proc. IEEE Trans. Intelligent Transportation Systems* vol 2 pp 1606–9
- [21] Mas J F and Flores J J 2008 The application of artificial neural networks to the analysis of remotely sensed data *Int. J. Remote Sens.* **29** 617–63
- [22] Huang G B 2003 Learning capability and storage capacity of two-hidden-layer feedforward networks *IEEE Trans. Neural Netw.* **14** 274–81
- [23] Stathakis D 2009 How many hidden layers and nodes? *Int. J. Remote Sens.* **30** 21–33
- [24] Storn R and Price K 1997 Differential evolution—a simple and efficient heuristic for global optimization over continuous space *J. Glob. Optim.* **11** 341–59
- [25] Chen J and Huang H 2002 *Sensors and Measurement Technologies* (Beijing: Higher Education Publishing Press) (in Chinese)
- [26] Heidenhain 2010 Technical description of angle encoders with integral bearing (http://www.heidenhain.com/en_US/php/documentation-information/documentation/brochures/popup/media/media/file/view/file-0022/file.pdf)